Deriving a Frozen Area Fraction From Metop ASCAT Backscatter Based on Sentinel-1

Helena Bergstedt, Annett Bartsch, Anton Neureiter, Angelika Höfler, Barbara Widhalm, Nicholas Pepin, and Jan Hjort

***Abstract*— Surface state data derived from spaceborne microwave sensors with suitable temporal sampling are to date only available in low spatial resolution (25–50 km). Current approaches do not adequately resolve spatial heterogeneity in landscape-scale freeze–thaw processes. We propose to derive a frozen fraction instead of binary freeze–thaw information. This introduces the possibility to monitor the gradual freezing and thawing of complex landscapes. Frozen fractions were retrieved from Advanced Scatterometer (ASCAT, C-band) backscatter on a 12.5-km grid for three sites in noncontinuous permafrost areas in northern Finland and the Austrian Alps. To calibrate the retrieval approach, frozen fractions based on Sentinel-1 synthetic aperture radar (SAR, C-band) were derived for all sites and compared to ASCAT backscatter. We found strong relationships for ASCAT backscatter with Sentinel-1 derived frozen fractions (Pearson correlations of −0.85 to −0.96) for the sites in northern Finland and less strong relationships for the Alpine site (Pearson correlations −0.579 and −0.611, including and excluding forested areas). Applying the derived linear relationships, predicted frozen fractions using ASCAT backscatter values showed root mean square error (RMSE) values between 7.26% and 16.87% when compared with Sentinel-1 frozen fractions. The validation of the Sentinel-1 derived freeze–thaw classifications showed high accuracy when compared to *in situ* near-surface soil temperature (84.7%–94%). Results are discussed with regard to landscape type, differences between spring and autumn, and gridding. This article serves as a proof of concept, showcasing the possibility to derive frozen fraction from coarse spatial resolution scatterometer time series to improve the representation of spatial heterogeneity in landscape-scale surface state.**

***Index Terms*— Advanced Scatterometer (ASCAT), freeze–thaw, permafrost, Sentinel-1, surface state.**

Manuscript received June 20, 2019; revised October 7, 2019 and November 11, 2019; accepted December 28, 2019. Date of publication March 13, 2020; date of current version August 28, 2020. This work was supported by the Austrian Science Fund [Fonds zur Förderung der Wissenschaftlichen Forschung (FWF)] through the Doctoral College GIScience under Grant DK W1237-N23. The work of Annett Bartsch was supported in part by the ESA's DUE GlobPermafrost Project under Contract 4000116196/15/I-NB, in part by the Zentralanstalt für Meteorologie und Geodynamik (ZAMG) Entwicklungsprojekt under Grant Sen4Austria, and in part by the ESA CCI+ Permafrost. The work of Anton Neureiter, Angelika Höfler, and Barbara Widhalm was supported in part by the ESA's DUE GlobPermafrost Project under Contract 4000116196/15/I-NB and in part by the ZAMG Entwicklungsprojekt under Grant Sen4Austria. The work of Jan Hjort was supported by the Academy of Finland Project under Grant 315519. *(Corresponding author: Helena Bergstedt.)*

Helena Bergstedt was with the Department of Geoinformatics-Z_GIS, University of Salzburg, 5020 Salzburg, Austria, and also with the Austrian Polar Research Institute, 1300 Vienna, Austria. She is now with the Water and Environmental Research Center, Institute of Northern Engineering, University of Alaska Fairbanks, Fairbanks, AK 99775 USA (e-mail: hbergstedt@alaska.edu).

Annett Bartsch is with b.geos, 2100 Korneuburg, Austria, and also with the Austrian Polar Research Institute, 1300 Vienna, Austria.

Anton Neureiter and Angelika Höfler are with the Department for Climate Research, Zentralanstalt für Meteorologie und Geodynamik (ZAMG), 1190 Vienna, Austria.

Barbara Widhalm is with the Staff Unit Earth Observation, Zentralanstalt für Meteorologie und Geodynamik (ZAMG), 1190 Vienna, Austria.

Nicholas Pepin is with the Department of Geography, University of Portsmouth, Portsmouth PO1 3HE, U.K.

Jan Hjort is with the Geography Research Unit, University of Oulu, 90014 Oulu, Finland (e-mail: jan.hjort@oulu.fi).

Color versions of one or more of the figures in this article are available online at http://ieeexplore.ieee.org.

Digital Object Identifier 10.1109/TGRS.2020.2967364

I. Introduction

LARGE parts of the Earth's surface are characterized by seasonal freezing and thawing processes. These processes are especially important for the higher latitudes and mountainous areas that are largely underlain by perennially frozen ground (permafrost). Seasonal freezing and thawing cycles have been shown to be an important driver of hydrological [1] and ecological processes [2]. Accurate knowledge about the extent, depth, and timing of freeze and thaw is an asset for modeling approaches of climate, surface energy balance, permafrost hydrology, and greenhouse gas emissions such as methane (e.g., [3], [4]).

Multiple data sets containing surface state information derived from microwave remote sensing have been published in the past (e.g., [5], [6]). Microwave remote sensing has been used for freeze–thaw retrieval in permafrost areas using different approaches and data sources [7]–[10]. Both active and passive microwave remote sensing platforms have been employed to create algorithms and data products tailored to monitoring of the ground surface state of high latitude regions (e.g., [11]–[13]). The freeze–thaw retrieval algorithms based on active systems [e.g., on the Advanced Scatterometer (ASCAT)] utilize the dependence of microwave backscatter on the dielectric constant of water contained within the ground. The dielectric constant itself is influenced by the state of water (frozen or liquid) contained in the ground and causes the backscatter to change in relation to the freeze–thaw of the ground surface. Scatterometers, such as the ERS scatterometer or the NASA Scatterometer (NSCAT) (see [14]–[16]) as well as Metop ASCAT (C-band) [10], have been successfully used to retrieve and monitor freeze–thaw information in the Arctic on a circumpolar scale. Due to its high temporal resolution (approximately daily observations), ASCAT has shown its potential for the monitoring of freeze–thaw cycles [10]. This data set has been demonstrated to be of value for the estimation of mean annual ground temperature in permafrost regions [17]. The coarse spatial resolution of scatterometer

observations (25–50 km) does not allow for freeze–thaw monitoring with rich spatial details. Synthetic aperture radar (SAR) C-band instruments have been used for freeze–thaw monitoring in Arctic environments and have been shown to be applicable to freeze–thaw monitoring in multiple studies (e.g., [13], [18], [19]). Attention has also been paid to freeze–thaw retrieval in the mid-latitudes (e.g., [20]). SAR instruments have a much higher spatial resolution (e.g., 10 m for Sentinel-1) in contrast to the comparatively low spatial resolution of scatterometer sensors (e.g., 25 km for ASCAT). However, most available SAR platforms in the past offered only infrequent observations [13]. This did, so far, not allow for high temporal resolution and high spatial resolution analysis or near-real-time monitoring of highly dynamic freeze–thaw cycles during transitional periods. Comparisons of freeze–thaw data sets from scatterometer and SAR sensors reveal significant differences in complex landscapes that are either mountainous or lake-rich Arctic environments [21].

Although freeze–thaw information retrieved using ASCAT time series is binary information (either a grid cell is frozen or thawed), the backscatter signal itself shifts over time from the average winter to summer value (see Fig. 6). Studies have theorized that the gradual rise and fall in backscatter could be linked to an increase or decrease in the fraction of frozen surface area within the respective ASCAT grid cell (see [21], [22]). It has been observed that the thawing process within one ASCAT grid cell can last a full month (shown for a study site in Alaska) [21]. A gradual shift occurring in L-band SMOS brightness temperature has been linked to change in the depth of the freezing front that gradually increases or decreases over time during the transitional periods [23].

In this article, we investigate the gradual rising and falling of backscatter values during transitional periods using scatterometer observations from ASCAT as well as SAR data sets from the Sentinel-1 constellation. We hypothesize that contrary to current literature, a gradual shift in freezing (or thawing) of the ground surface of the area contained within the respective ASCAT grid cell can be quantified instead of a binary approach. Furthermore, we present an approach to derive a fraction of frozen–thawed area per ASCAT grid cell instead of the currently available binary, frozen/unfrozen surface state information.

II. Data and Study Sites

A. Remote Sensing Data Sets

This article focuses on the C-band (5.2 GHz) VV-polarized backscatter data sets from the ASCAT onboard the Metop satellites. It offers a spatial resolution of 25–50 km [24]. Backscatter data used in this article are provided by EUMETSAT in a 12.5-km grid as part of the soil moisture data product. The provided backscatter value has been normalized to a 40° incidence angle. Data are continuously available since 2007, providing global coverage with a temporal resolution of approximately daily observations [25].

To be able to account for spatial variability in the freeze–thaw process, we utilize Sentinel-1 C-band (5.4 GHz) backscatter data. In this article, we employ data obtained in interferometric wide (IW) swath mode, as it is the predefined mode over land areas. The Copernicus Sentinel-1 data were obtained from the Alaska Satellite Facility's (ASF) data portal Vertex as Level-1 Ground Range Detected High Resolution dual polarization products (GRD-HD, 10 × 10 m pixel spacing). To ensure the best possible comparability between ASCAT and Sentinel-1 observations, this analysis was limited to the V-polarized bands of the Sentinel-1 data set.

Landcover is expected to influence the retrieval of freeze–thaw information (e.g., [21]). Sentinel-2 multispectral observations from July to August 2018 were used for landcover classifications to mask out several landcover classes (e.g., water, bedrock, and glaciers) from the analysis of Sentinel-1 data. Sentinel-2A and 2B carry the Multispectral Instrument (MSI) orbiting the Earth at 786-km altitude. The spatial resolution varies among the spectral bands and ranges from 10 m for the visible and the broad near infrared (NIR) bands, 20 m for the red edge, narrow NIR and short wave infrared (SWIR) bands, and 60 m for the atmospheric bands. The bands 3 (green, 10 m), 4 (red, 10 m), 8 (NIR, 10 m), 11 (SWIR, 20 m), and 12 (SWIR, 20 m) have been shown to be applicable, especially to Tundra and Arctic environments and were, therefore, used in this analysis [26].

B. Study Sites

We focus on three study sites for which distributed near-surface temperature measurements could be obtained (Table I). They are affected by seasonal frost and noncontinuous permafrost (sporadic or isolated). All study sites further feature different shares of forested as well as sparsely vegetated areas, bare rock, and boulder landforms. Additionally, all sites include surface water in the form of lakes and rivers. Each study site is approximately the size of one ASCAT grid cell of the ASCAT soil moisture data product by EUMETSAT gridded to 12.5 km.

Two study sites for this analysis, the Kevo and Kaldoaivi sites, are located in northern Finland near and around the Kevo Subarctic Research Station. The sites differ significantly from the third one in the complexity of the terrain and the difference in elevation within the grid cell (see Fig. 1). The Kevo and Kaldoaivi sites differ in the amount of forested area. The Kevo site features more and denser forest cover as well as a larger river and a lake system (Kevojärvi) compared to the Kaldoaivi site.

The third study site is located in the Hohe Tauern National Park in the Austrian Alps around the Hoher Sonnblick mountain. This site features multiple glaciers as well as areas of permanent or multiyear snow cover.

C. In Situ Observations

Air temperature measurements for all study sites were used to determine the backscatter thresholds for the freeze–thaw algorithm. Air temperature measurements for the Hohe Tauern site were obtained from the Zentralanstalt für Meteorologie und Geodynamik (ZAMG) and were available in 10-min resolution for the entire study period from 2016 to 2018 [29]. The air temperature measurements for the Hohe Tauern site

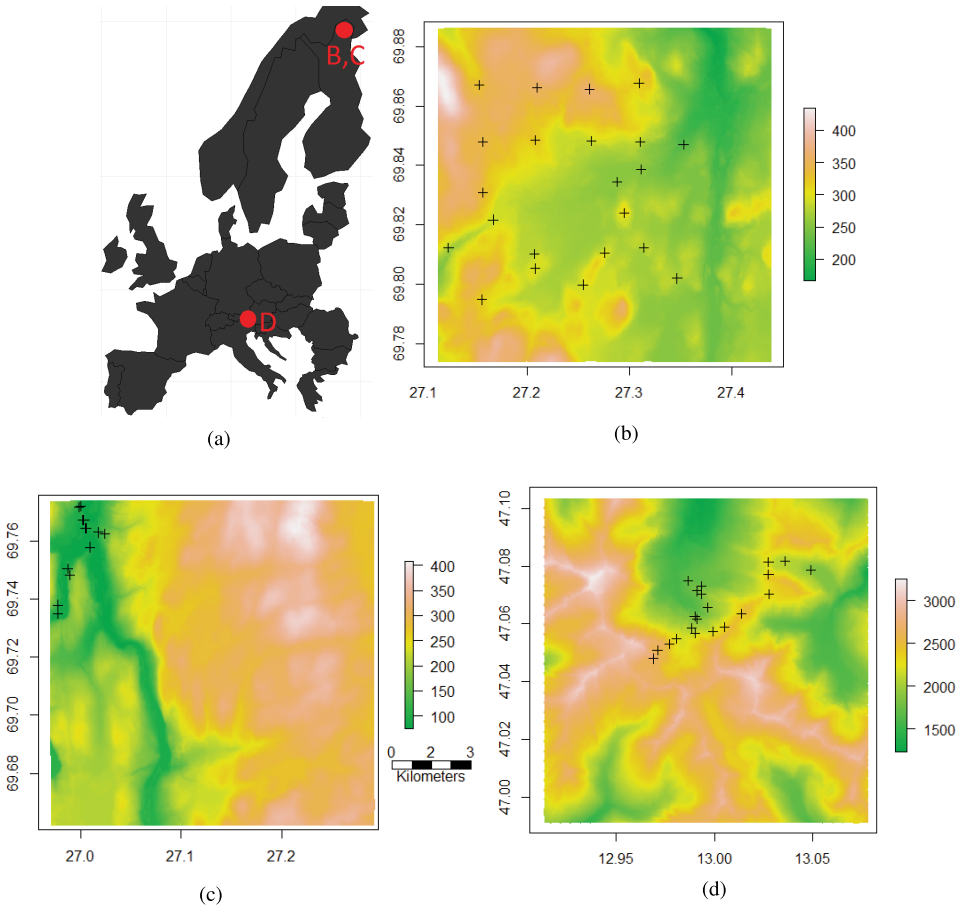

Fig. 1. Map showing an (a) overview of the three study sites as well as detailed maps of (b) Kaldoaivi, (c) Kevo, and (d) Hohe Tauern sites showing DEMs (data sources: [27], [28]) with elevation in meter above sea level; including the distribution of measurement points for *in situ* near-surface ground temperature.

were obtained from the Hohe Sonnblick observatory located on a summit within the grid cell.

Air temperature measurements for the Kaldoaivi site (Finland) were acquired via an automated weather station. In addition to the air temperature measurements, this site offered borehole ground temperature measurements from depths of 0.5, 0.75, and 1 m. This site is located at the well-studied palsa site in the Vaisjeaggi palsa mire (e.g., [30], [31]). This site used Onset TMC-HD temperature sensors and HOBO8 U12 data loggers for both air and ground temperature. However, as the air temperature from this location observations did not cover the time period of interest to a sufficient amount, final calibration of the freeze–thaw detection (determination of thresholds) for the Kaldoaivi grid cell was done using the air temperature measurement from the measurement site located in the Kevo grid cell. This site is located approximately 5 km west from the Kaldoaivi grid cell.

For the Kevo study site, air temperature measurements were obtained from the measurement station located at the Kevo Subarctic Research Station, located near the center of the respective grid cell. The data set was obtained through the National Oceanic and Atmosphere Administration (NOAA) National Centers for Environmental Information data portal.

Near-surface ground temperature *in situ* measurements for all study sites were used to verify and validate the results obtained from the remote sensing data analysis. Extensive near-surface soil temperature measurements were performed from summer 2016 to summer 2018 in the Hohe Tauern site (Austria) and the Kaldoaivi site (Finland). Temperature measurements were obtained by distributing iButton temperature loggers to cover different landscape types in the grid cells and different elevations (for more details see Table II). The iButton loggers were placed approximately 2–3 cm below the surface to avoid direct warming influence by the Sun.

Near-surface temperature measurements in the Kevo site were measured at 2-cm depth by Pendant UA-002-64/TidbiT v2 dataloggers every 30 min. Continuous data were recorded from 17 September 2011 to 31 August 2018. Most sites were in soil/vegetated areas. Sites used in this article range from lakeside (80 m above sea level) to freely draining slope sites (146 m above sea level).

Additional *in situ* data have been collected in the Hohe Tauern area in order to determine the accuracy of the adapted landcover classification scheme. As this classification targets the separation of areas with bedrock, special emphasis was on collecting information from bedrock/boulder (25 data points) versus soil/vegetation (18 points) covered areas.

TABLE I

OVERVIEW OF STUDY SITES (GRID CELLS) INCLUDING LOCATION, SURFACE WATER FRACTION, FRACTION OF PERMANENT SNOWCOVER/GLACIERS, FRACTION OF BEDROCK/BOULDERS AS GIVEN BY THE LANDCOVER CLASSIFICATION. FRACTIONS GIVEN HERE ARE MASKED OUT FROM THE ANALYSIS

Study site	Latitude	Longitude	Surface water fr. %	Permanent snow/glacier fr. %	Bedrock/boulder fr. %
Hohe Tauern	47.05	12.99	1.65	4.59	36.7
Kevo	69.72	27.13	5.53	-	-
Kaldoaivi	69.83	27.27	3.42	-	-

TABLE II

OVERVIEW OF *In Situ* DATA SETS USED IN THIS ARTICLE

Grid cell	In situ measurement sites	Latitude	Longitude	measured Parameter
Kaldoaivi	Va-1 Vaisjeaggi1	69.82	27.17	Air temperature and ground temperature
Kaldoaivi	Kaldoaivi-iButtons	69.83	27.27	Near-surface ground temperature
Kevo	Utsjoki Kevo Kevojärvi	69.76	27.02	Air temperature
Kevo	Hobo Pendant/TidbiT	69.72	27.13	Near-surface ground temperature
Hohe Tauern	Hoher Sonnblick Observatory	47.05	12.96	Air temperature
Hohe Tauern	Hohe Tauern - iButtons	47.05	12.99	Near-surface ground temperature

III. METHODOLOGY

A. Sentinel-1 Preprocessing

Sentinel-1 GRD-HD was preprocessed using the Sentinel Application Platform (SNAP) toolbox. In SNAP, Sentinel-1 data were subjected to the application of the orbit file, thermal noise removal, calibration, terrain correction, and the conversion to decibel (dB). For the terrain correction, we applied high-resolution digital elevation models (DEM) for both the study site in Austria and the study sites in Finland. For Austria, we used a 10-m spatial resolution derived from laser scanning data from 2015 published by the state of Salzburg (Austria) [27]. For both study sites in Finland, DEMs of different spatial resolutions are available (2 and 10 m). To have comparable data sets for all study sites, all analyses were performed on data preprocessed using 10-m DEMs [28]. The DEM for Finland is based on topographic data published by the National Land Survey of Finland with a 1.4-m elevation accuracy [28]. Sentinel-1 data were normalized to a 40° incidence angle (in accordance with the ASCAT backscatter being normalized to this incidence angle) using the methodology presented in [32].

B. Landcover Classification

To distinguish different landcovers within the selected grid cells, we created landcover classifications for all selected study sites. For landcover classifications regarding the Kaldoaivi and Kevo sites, we followed the classification approach presented in [33] which was specifically developed for Arctic and permafrost environments. As input data, Sentinel-1 observations (VV-pol, IW mode) from December 2017 were combined with Sentinel-2 acquisitions from July/August 2018. We performed a maximum likelihood classification based on the signatures published in [33]. They represent the modified results of an unsupervised classification (k-means). This landscape classification offers 21 possible classes including sparse vegetation, different shrub types, forests as well as different water classes of which the three water classes have been used for masking in this analysis. This classification approach also offers grouped classes that are used to simplify the visualization (see Fig. 2). The accuracy of the classification approach presented in [33] was determined using *in situ* vegetation data from central Yamal (tundra over continuous permafrost) and the northern Ural region (taiga–tundra transition zone over discontinuous permafrost) [34]. Bartsch *et al.* [34] reported an agreement on the vegetation classification with the *in situ* data of 70%–94.1%.

For the Hohe Tauern area, this classification scheme has been adapted to Alpine environments that also include extensive bedrock and boulder areas as well as glaciers and permanent snowfields. Both polarization combinations available from Sentinel-1 (VV and VH) have been used to exploit the polarization-dependent backscatter response. Summer data (July 2017) in addition to acquisition from frozen conditions across the entire area of interest (January 2017) have been included for the k-means classification. This results in 19 classes including bedrock areas that are required for masking of areas with too low water content. As the employed algorithm relies on the backscatter changes caused by the changing dielectric constant of the water contained in the ground, these areas are not sensitive to this kind of backscatter change.

C. Compatibility of ASCAT and Sentinel-1

To demonstrate the compatibility of ASCAT and Sentinel-1 for freeze–thaw retrieval applications, we compared the ASCAT backscatter time series with resampled Sentinel-1 backscatter time series. For this purpose, Sentinel-1 mean values were calculated for each available acquisition from all pixels contained within the respective ASCAT grid cell. This was done for all grid cells used in this article. The created Sentinel-1 mean value time series were compared to the respective ASCAT time series visually (see Fig. 4), and by their Pearson correlation for acquisition dates where values for both Sentinel-1 and ASCAT were available.

D. Freeze–Thaw Retrieval Algorithm

The freeze–thaw algorithm used in this article was published by Naeimi *et al.* [10] as the ASCAT surface state flag in conjunction with the soil moisture algorithm for ASCAT.

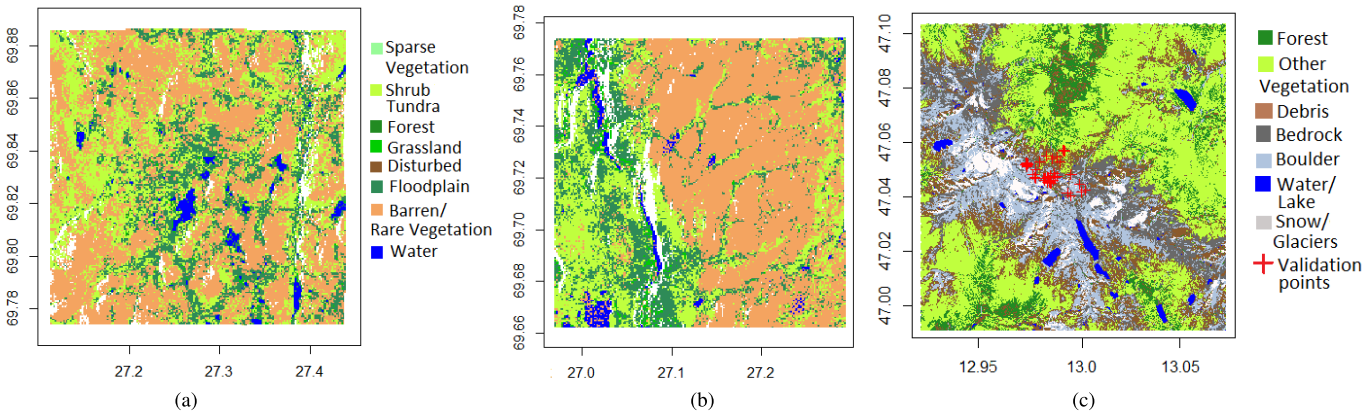

Fig. 2. Detailed maps of the landcover classifications for (a) Kaldoaivi, (b) Kevo, and (c) Hohe Tauern sites including the distribution of validation points in the case of the Hohe Tauern study site (c). For the Hohe Tauern site (c) points that were used for validation for the landcover classification are displayed. White areas in (a) and (b) are areas of no data. Legend of (a) is valid for (a) and (b).

It was designed to derive the surface state and monitor freeze–thaw events and was validated using surface temperature and near-surface temperature measurements in Siberia and Alaska as well as with air temperature from World Meteorological Organization (WMO) meteorological stations and modeled soil temperature data sets [ECMWF ReAnalysis (ERA-Interim) and Global Land Data Assimilation System (GLDAS)-Noah]. Naeimi *et al.* [10] reported an overall accuracy between 80.26% and 91.79% for the comparison with *in situ* soil temperature data, an overall accuracy of 81.93% for the comparison with air temperature and an overall accuracy with modeled soil temperatures of 83.09% and 83.86% for ERA-Interim and GLDAS-Noah, respectively. The reported accuracy for the different data sets was different for frozen, unfrozen, and transitional periods [10]. The algorithm classifies ASCAT backscatter values into frozen, unfrozen, unknown, and snowmelt/water on the surface using backscatter thresholds. The thresholds are obtained through collocating the backscatter data with the near-surface soil temperature from the ERA-Interim data set due to the limited availability of *in situ* data on a global scale. The backscatter level at the freeze–thaw point (σ^0FTL, the blue line in Fig. 3) is determined as the inflection point of a logistic function fit to ASCAT backscatter collocated with ERA-Interim soil temperature data (red curve in Fig. 3). An example of this is shown in Fig. 3. In addition to the backscatter level of the freeze–thaw transition, the algorithm relies on the mean backscatter during the summer months (σ^0SM) and the backscatter at the snowmelt level (σ^0SML, the green line in Fig. 3). Naeimi *et al.* [10] have reported the best results of this process if the regression is limited to values between +10 °C and −10 °C. This approach has been reported to be applicable for Arctic regions.

In this article, instead of reanalysis data, we could employ air temperature measurements obtained within or near the studied grid cells for the extraction of the model parameters. Naeimi *et al.* [10] reported similar validation results of their surface state data product compared with modeled soil temperature (83.09%) and air temperature data (81.93%). By focusing on available *in situ* information, we avoid possible uncertainties associated with reanalysis data sets.

E. Quantifying Partial Freezing

To investigate the gradual rise and fall of ASCAT backscatter values during transitional periods Sentinel-1 backscatter was used to resolve spatial differences in freeze–thaw transitions within one ASCAT grid cell. To calculate the frozen fraction per ASCAT grid cell (fraction of frozen pixel) Sentinel-1 was classified following the same freeze–thaw retrieval algorithm as introduced for ASCAT [10].

Sentinel-1 data were classified in frozen/unfrozen according to the freeze–thaw retrieval algorithm on a pixelwise basis. To decrease processing times Sentinel-1 data were resampled to a 40-m pixel spacing from the original 10 × 10 m grid. The classification of the Sentinel-1 time series was validated using the *in situ* near-surface ground temperature measurements described in Section II-C.

Landscape types associated with temporal or permanent surface water coverage were masked out before the freeze–thaw retrieval. Backscatter changes caused by freeze–thaw transitions are linked to the state change of water contained within the near-surface ground. Landscape types known to be nonsensitive to this kind of backscatter change due to a lack of near-surface water content of the ground (e.g., bedrock and large boulders) were masked from the analysis. For the Alpine site landscape type glaciers and multiyear snow cover were masked as well due to their different backscattering behavior over time. Percentages of masked areas are documented in Table I.

The resulting frozen fraction is expected to be linearly related to the ASCAT backscatter of the corresponding grid cell. Deviations may occur due to the omission of water and snow areas in the Sentinel-1 time series. Following this assumption, we performed a linear regression of values for frozen fraction and ASCAT backscatter for 75% of the available data. The created linear equation was used to calculate frozen fractions from ASCAT backscatter values for the remaining 25% of the data set aside for validation. The data were separated randomly into 75% and 25% to avoid bias due to different years showing different numbers in Sentinel-1 acquisitions. To avoid the influence of snowmelt on the correlation and the calculation of frozen fraction from

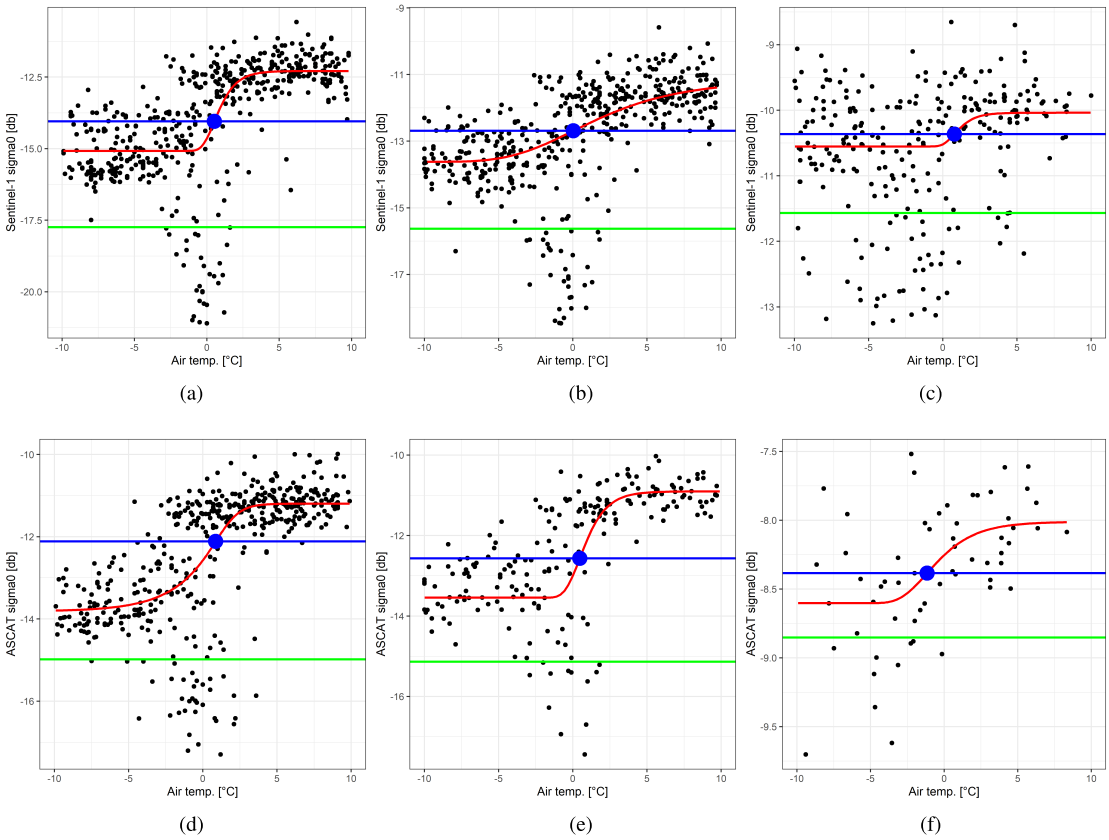

Fig. 3. Example of Sentinel-1 backscatter (σ^0, footprint average) and ASCAT backscatter versus air temperature data (source: station located at the Kevo Subarctic Research Station; obtained through the NOAA and from the ZAMG) for (a) and (d) Kaldoaivi, (b) and (e) Kevo, and (c) and (f) Hohe Tauern sites. Air temperature for Hohe Tauern site measured on Hohe Sonnblick summit within the footprint. The red curve indicates the best fit logistic function. The blue line indicates the inflection point of the fit logistic function which is assumed to represent the backscatter of the freeze–thaw transition level. The green line indicates the snowmelt level.

ASCAT backscatter, days with detected snowmelt conditions in ASCAT backscatter were excluded from the correlation analysis. To verify the validity of this classification, we compared the retrieved surface state with near-surface ground temperature time series.

It is known that forested areas cause uncertainties in surface state retrieval with C-band backscatter (e.g., [13]). In our study, the Hohe Tauern site shows areas of dense forest in areas with low elevation included in the analyzed grid cell. To quantify the influence of the forested areas on the overall result, the analysis was done including as well as excluding these areas to be able to compare the results.

F. Validation of Freeze–Thaw Classification

To verify the Sentinel-1 freeze–thaw classification, which is the basis for quantifying the frozen fraction, classification results were compared to *in situ* near-surface ground temperature measurements for all three study sites. For comparison, the Sentinel-1 backscatter time series for the pixels of all available *in situ* measurement locations were extracted and classified separately. To quantify the agreement of the classification and the *in situ* measurements, classification results were separated into frozen, unfrozen, and melting periods and compared to *in situ* data from the corresponding time periods. This was visualized in form of boxplots which represent descriptive statistics including median, quartiles, and outliers.

IV. Results

A. Surface State Retrieval From Sentinel-1

A comparison of the ASCAT backscatter time series with resampled Sentinel-1 time series revealed high agreement of ASCAT and Sentinel-1 observation of the respective grid cells (see Fig. 4). Pearson correlations between ASCAT and resampled Sentinel-1 time series were high for the Kaldoaivi (0.97, 0.91) and Kevo sites (0.92, 0.89) for both ascending and descending acquisitions. The Hoher Tauern site showed slightly lower correlations with 0.55 and 0.70 for ascending and descending acquisitions, respectively. For all three study sites both ASCAT and the resampled Sentinel-1 time series showed the typical behavior of lower backscatter during winter months and higher backscatter during summer months with especially low backscatter values during periods of snowmelt (see Fig. 4). For the Kaldoaivi and Kevo sites, ASCAT shows very similar backscatter values compared to the resampled Sentinel-1 time series. While still following the typical temporal pattern, values of ASCAT and resampled Sentinel-1 are less similar for the Hohe Tauern site compared to the other two study sites (see Fig. 4). For the Kaldoaivi and Hohe Tauern

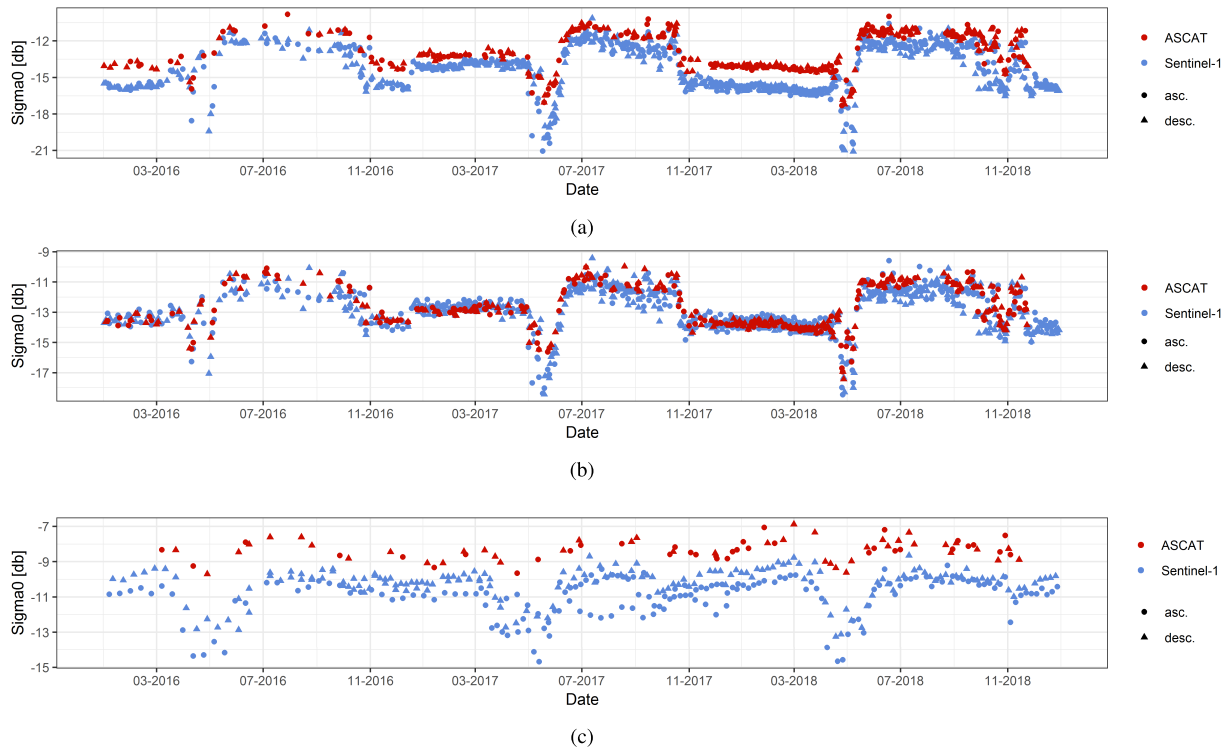

Fig. 4. Time series of ASCAT and Sentinel-1 backscatter (resampled to the ASCAT grid) for the three sites (a) Kaldoaivi, (b) Kevo, and (c) Hohe Tauern for the studied time period.

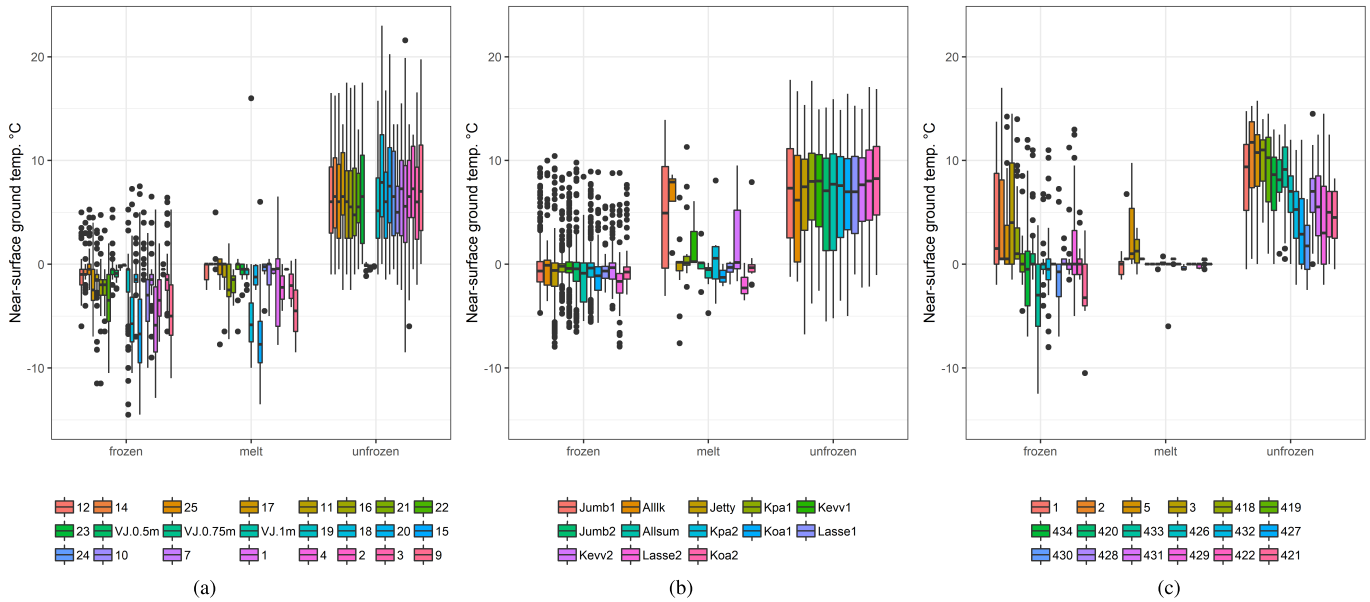

Fig. 5. Boxplots showing the agreement of *in situ* near-surface ground temperature time series with Sentinel-1-based pixelwise frozen, unfrozen, and melting snow conditions classification. Measurement points are sorted by elevation from low to high. Boxplots show median, quartiles, and outliers (black dots). Numbered measurement points represent locations instrumented with iButtons; Vaisjaeggi points (VJ) were instrumented with Onset TMC-HD temperature sensors and HOBO8U12 data loggers; named points at the Kevo location were instrumented with Pendant UA-002-64/TidbiTv2 dataloggers. (a) Kaldoaivi. (b) Kevo. (c) Hohe Tauern.

sites, ASCAT backscatter showed generally higher backscatter values compared to Sentinel-1.

To calculate the frozen fraction of ASCAT grid cells, the Sentinel-1 time series was classified as frozen/unfrozen using the threshold algorithm presented in [10]. The agreement of frozen/unfrozen from Sentinel-1 with near-surface ground temperature is 94% for the Kaldoaivi site, 87% for the Kevo site, and 84.7% or 85.6% for the Hohe Tauern site including and excluding forested areas, respectively. This is visualized in Fig. 5 which shows boxplots of classified

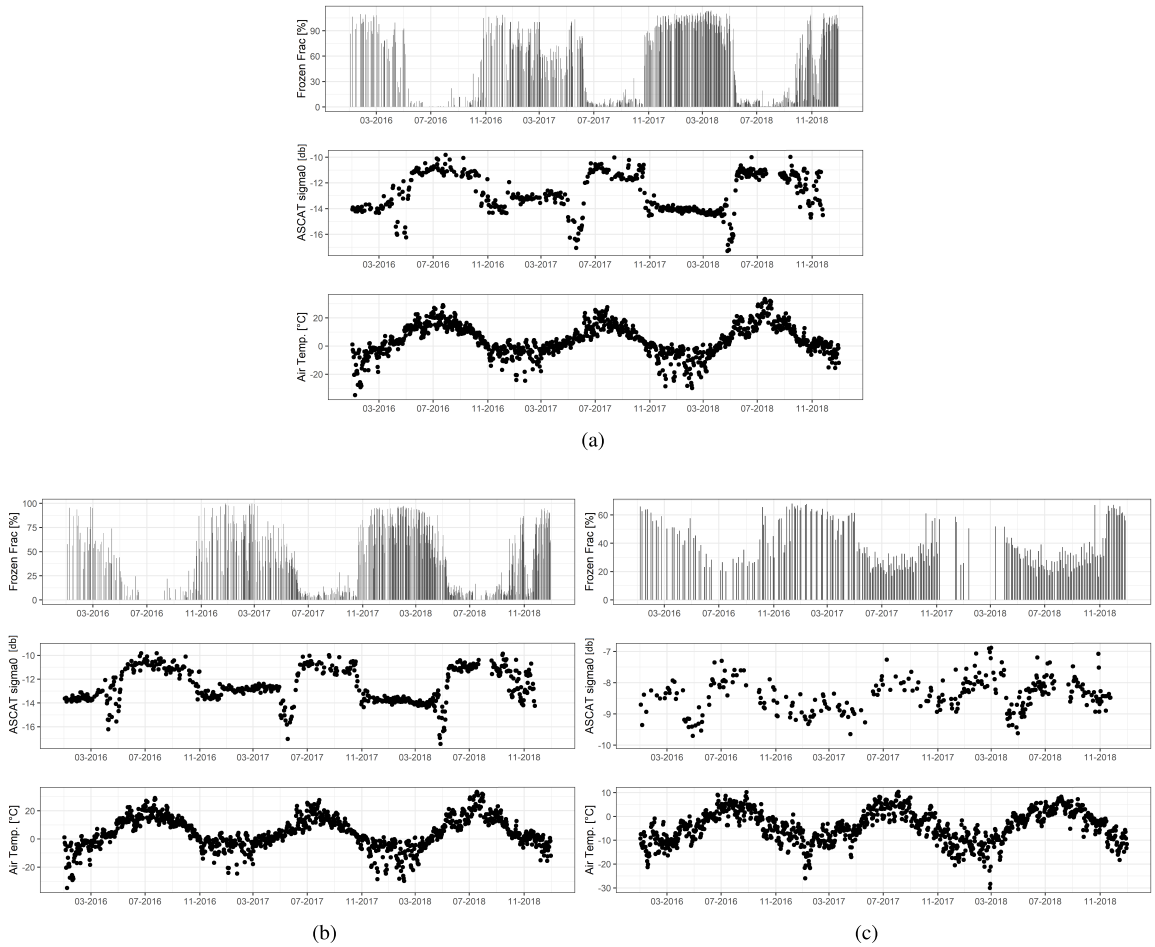

Fig. 6. Time series of Sentinel-1 frozen fraction, ASCAT backscatter and air temperature for study sites (a) Kaldoaivi, (b) Kevo, and (c) Hohe Tauern.

Sentinel-1 observations and the respective *in situ* near-surface ground temperature value for each *in situ* measurement location within the respective study site (Kaldoaivi, Kevo, and Hohe Tauern). For the Kaldoaivi and Kevo sites, median values of near ground surface temperature fall below 0 °C for all available *in situ* measurement points during periods classified as frozen using Sentinel-1 data (see Fig. 5). All *in situ* measurement points show outliers (black dots in Fig. 5) above 0 °C during the period classified as frozen by Sentinel-1 data. For the period classified as unfrozen using the Sentinel-1 time series, both the Kaldoaivi and Kevo sites exhibit median values between 5 °C and 10 °C for all available *in situ* measurement points. Comparison of *in situ* near–surface ground temperature measurements with frozen/unfrozen classification of Sentinel-1 data for the Hohe Tauern site shows several *in situ* measurement points with median temperatures above 0 °C during periods classified as frozen (see Fig. 5). Sites showing positive temperatures during as frozen classified periods are those that are forested and are situated at lower altitudes. Periods classified as melting snow from Sentinel-1 times series show *in situ* near-surface ground temperatures with values both above and below 0 °C for all three study sites.

The frozen fraction for all three study sites was calculated for all available Sentinel-1 acquisitions after masking with landcover. The classification accuracy for the landcover classification for bedrock at the Hohe Tauern site is 86% and 75% respectively (user accuracy and producer accuracy).

The resulting frozen fraction time series, as well as the corresponding ASCAT backscatter and air temperature time series, can be seen in Fig. 6. The time series of the frozen fraction follows the time series of both ASCAT backscatter and air temperature for all three sites (see Fig. 6). Differences between the sites lie in the maximum of the as-frozen classified fraction of the Sentinel-1 pixel. The Kaldoaivi and Kevo study sites show long periods (on and off for between November to May) of consistently high percentages of the frozen fraction (above 90% frozen) for all years considered in this article. The Hohe Tauern site shows lower overall frozen fractions as well as smaller differences between summer and winter levels of the frozen fraction (see Fig. 6). All three sites show differing amounts of frozen fractions during the summer months with the frozen fraction of the Hohe Tauern site exceeding the levels compared to the other sites.

B. ASCAT Backscatter Versus Frozen Fraction From Sentinel-1

The results of the linear regression for all three study sites, including the Pearson correlation coefficient values, are shown

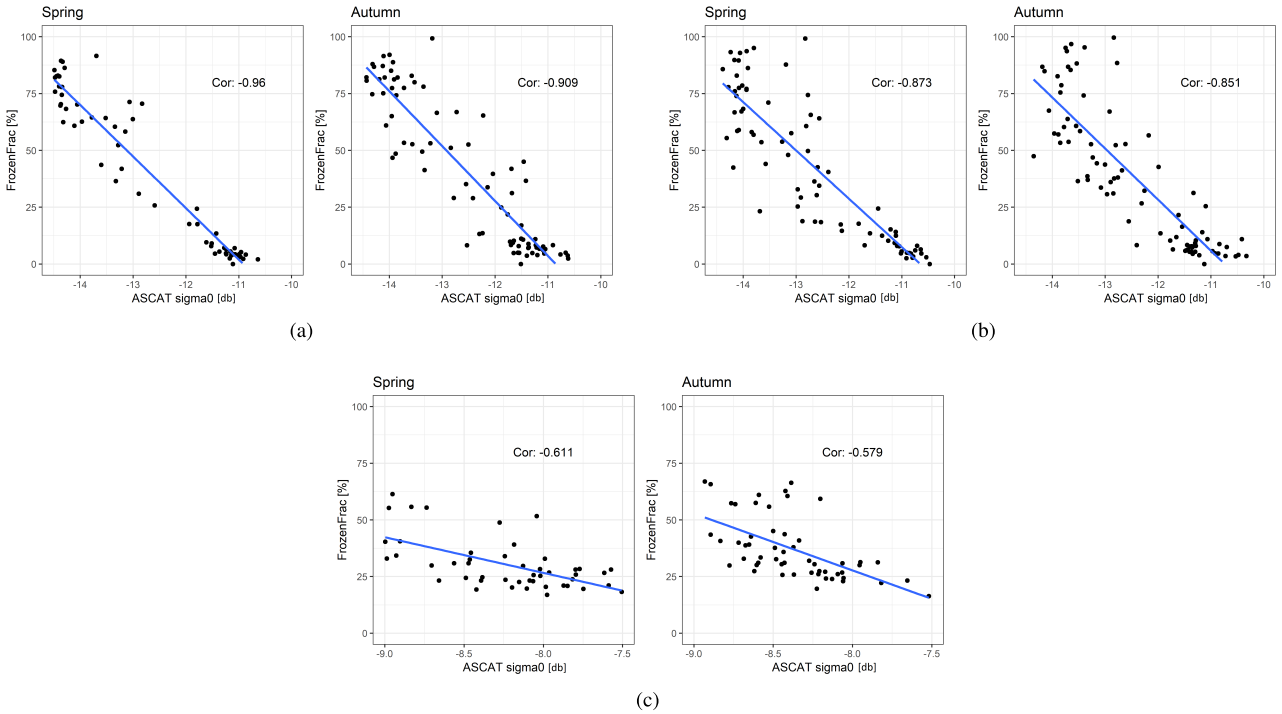

Fig. 7. Correlation (Cor.) of Sentinel-1 frozen fraction with ASCAT backscatter for study sites (a) Kaldoaivi, (b) Kevo, and (c) Hohe Tauern.

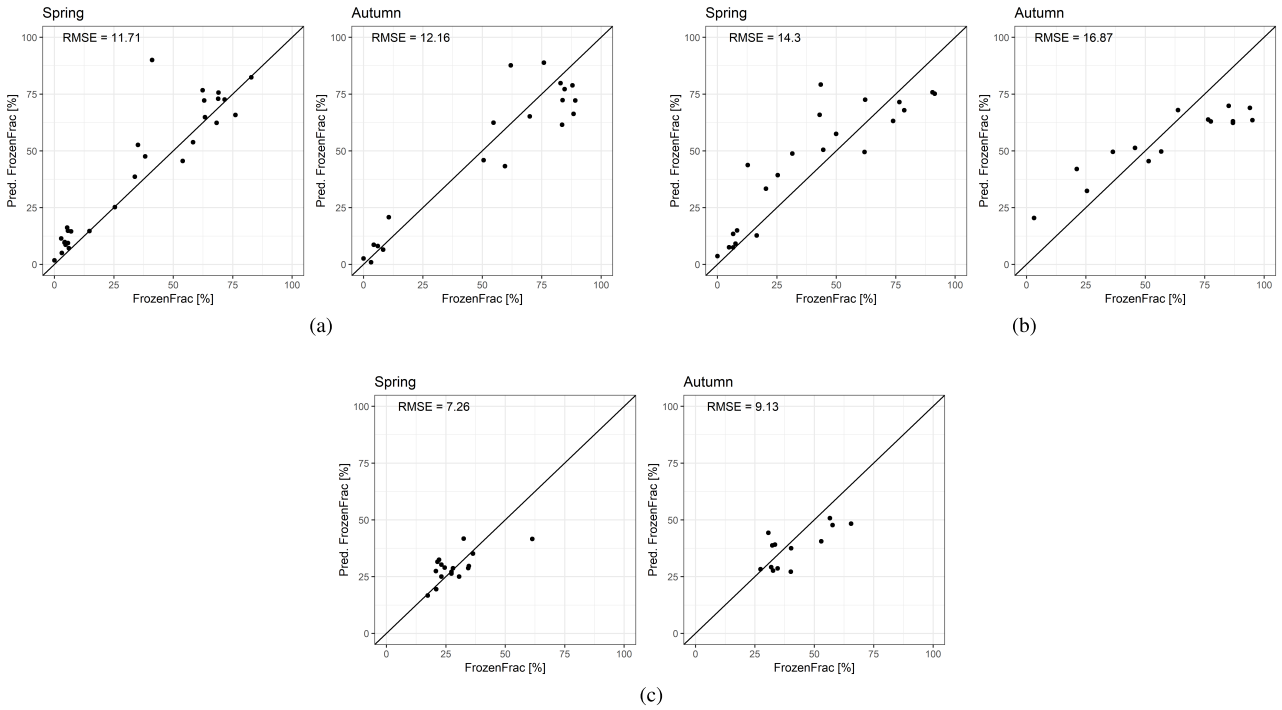

Fig. 8. Comparison of Sentinel-1 Frozen Fraction with predicted Frozen Fraction based on ASCAT backscatter for study sites (a) Kaldoaivi, (b) Kevo, and (c) Hohe Tauern. Solid black line represents 1:1 reference line.

in Fig. 7. For study sites Kaldoaivi and Kevo, strong negative Pearson correlations, −0.909 and −0.851, respectively, could be found for ASCAT backscatter and Sentinel-1 derived frozen fraction for freeze-up (autumn) periods (see Fig. 7). The Kaldoaivi and Kevo sites show similar strong negative correlations, −0.96 and −0.851 respectively, for the thaw period in spring (see Fig. 7). For the Hohe Tauern site, Pearson correlations are lower with −0.611 and −0.579, respectively, for spring and autumn (see Fig. 7).

To validate our results the equations obtained through linear regression (see Fig. 7) were applied to 25% of the data set aside for validation. Results show good agreement of

calculated and predicted frozen fraction for the Kaldoaivi and Kevo study sites. Both validations data sets for the Kaldoaivi and Kevo grid cells contain values for a range of frozen fractions from low values below 10% frozen area, to high frozen fractions of above 75% of the frozen area. During spring, the Kaldoaivi and Kevo sites show root mean square errors (RMSEs) of 11.71% and 14.3%, respectively (see Fig. 8). During autumn the Kaldoaivi and Kevo sites show higher RMSE values compared to spring of 12.15% and 16.97% respectively (see Fig. 8). The Hohe Tauern site shows a smaller range of frozen fraction compared to the Kaldoaivi and Kevo sites with RMSE values of 7.26% for spring and 9.13% for autumn (see Fig. 8).

V. Conclusion and Discussion

This article showed the possibility of utilizing the Sentinel-1 time series to calculate a frozen fraction per grid cell from ASCAT backscatter in different environments including mountain ranges.

Nevertheless, the results showed clear differences in accuracy for different study sites as well as within study sites. Validation of the threshold algorithm for surface state determination [10] applied to pixelwise Sentinel-1 time series shows good agreement between the freeze–thaw classification and the *in situ* near-surface temperature time series for all study sites with exception of measurement points within forested areas in the Alpine study site Hohe Tauern. Previous studies have also reported problems concerning freeze–thaw retrieval in forested areas via the C-band backscatter [13]. The overall agreement of *in situ* measurements with the surface state as determined by the threshold algorithm (between 84% and 94%) is slightly higher to values reported in [10] between (80% and 92%). Although the overall agreement between near-surface ground temperature measurements and the freeze–thaw classification was high, outliers (black dots in Fig. 5) for all measurement points were evident. Even though the high spatial resolution of Sentinel-1 (gridded to 40 m in this article) brings clear improvement compared to the coarse spatial resolution of ASCAT, small scale local heterogeneity in freeze–thaw progression as caused by vegetation, snow or ground properties cannot be fully captured and lead to differences between field and remote sensing observations.

As certain landcover types (e.g., bedrock) are not sensitive to backscatter changes due to freeze–thaw processes, these areas have been masked from the analysis of Sentinel-1. Due to their nonsensitivity, these areas are assumed to have only negligible influence on the ASCAT freeze–thaw retrieval; however, this does not hold for other masked out areas such as water bodies. Here, it can be assumed that the influence of water bodies that is avoided in the Sentinel-1 analysis through masking, influences the freeze–thaw retrieval using ASCAT backscatter. This will also have an impact on the found relationship between Sentinel-1 derived frozen fraction and ASCAT backscatter and with that on the accuracy of the frozen fraction derived from ASCAT backscatter. Our results highlight the need for site-specific calibration of freeze–thaw retrieval approaches as well as the importance of high quality landcover information. Additionally, differences between thawing and freeze-up periods are evident and require separate calibration and analysis.

This analysis is focused on ASCAT data gridded to 12.5 km and not on the shape or resolution of the original ASCAT footprint. As the 12.5-km grid is widely used (e.g., [10], [17], [35], [36]), it was chosen to make our results comparable to existing literature. The difference between the geometry and resolution of the grid used in our analysis and the original ASCAT footprint is likely impacting the accuracy of our results. This may also influence the slight differences between ASCAT and Sentinel-1 backscatter as shown in Fig. 4. ASCAT backscatter is also available in other grid spacings and higher spatial resolutions (e.g., 4.45-km grid spacing in [37]) and utilizing these kinds of data sets is likely to improve the accuracy of the derived frozen fraction in future analysis. The air temperature data used for parameterization in this article are not available in high resolution similar to the near-surface ground temperature measurements. The assumption that air temperature data from one measurement location is representative of a 12.5-km ASCAT grid cell might contribute to uncertainties in deriving the thresholds used for freeze–thaw retrieval, especially for the Hohe Tauern site.

Other factors such as temporal changes in surface roughness, in the vertical distribution of the frost front and temporal changes in moisture of vegetation and soil also influence the behavior of backscatter and may contribute to the lower accuracy in some locations as well as the observed RMSE of our results.

The difference in the timing of ascending and descending acquisitions may also influence the accuracy of our results. During transitional periods where the surface state might vary on a daily basis (thawing with higher temperatures at midday and re-freezing at night) the difference in acquisition timing contributes to the uncertainty of the derived surface state information.

Currently, this analysis is limited to three sites in the Subarctic and the Austrian Alps. Although these sites show a wide range of surface types and were specifically instrumented for this analysis, an extension of this research to additional locations would be beneficial for further understanding. In particular, future studies in high Arctic environments would contribute to strengthening this approach.

The ASCAT-derived frozen fraction has the potential to improve monitoring of freeze–thaw transitions in tundra areas on a circumpolar scale. The high temporal resolution of ASCAT allows for daily monitoring of the circumpolar surface state and the improved spatial information through the introduction of the frozen area fraction aided by high resolution Sentinel-1 data facilitates the more detailed observation of the progression of surface state change on a landscape scale.

References

[1] G. Wang, H. Hu, and T. Li, "The influence of freeze–thaw cycles of active soil layer on surface runoff in a permafrost watershed," *J. Hydrol.*, vol. 375, nos. 3–4, pp. 438–449, Sep. 2009.

[2] T. Zhang, R. G. Barry, and R. L. Armstrong, "Application of satellite remote sensing techniques to frozen ground studies," *Polar Geography*, vol. 28, no. 3, pp. 163–196, Jul. 2004.

[3] M. Mastepanov *et al.*, "Large tundra methane burst during onset of freezing," *Nature*, vol. 456, no. 7222, pp. 628–630, Dec. 2008.

[4] M. Mastepanov *et al.*, "Revisiting factors controlling methane emissions from high-arctic tundra," *Biogeosciences*, vol. 10, no. 7, pp. 5139–5158, Jul. 2013.

[5] C. Paulik *et al.*, "Circumpolar surface soil moisture and freeze/thaw surface status remote sensing products (version 4) with links to geotiff images and NetCDF files (2007-01 to 2013-12)," Dept. Geodesy Geoinformatics, TU Vienna, Vienna, Austria, 2014, doi: 10.1594/PANGAEA.832153.

[6] D. Sabel, S.-E. Park, A. Bartsch, S. Schlaffer, J.-P. Klein, and W. Wagner, "Regional surface soil moisture and freeze/thaw timing remote sensing products with links to geotiff images," *PANGAEA*, 2012, doi: 10.1594/PANGAEA.779658.

[7] Y. Kim, J. S. Kimball, K. C. McDonald, and J. Glassy, "Developing a global data record of daily landscape Freeze/Thaw status using satellite passive microwave remote sensing," *IEEE Trans. Geosci. Remote Sens.*, vol. 49, no. 3, pp. 949–960, Mar. 2011.

[8] K. C. McDonald and J. S. Kimball, "Estimation of surface freeze–thaw states using microwave sensors," in *Encyclopedia of Hydrological Sciences*, M. G. Anderson and J. J. McDonnell, Eds. Wiley Online Library, 2006, doi: 10.1002/0470848944.hsa059a.

[9] H. Park, Y. Kim, and J. S. Kimball, "Widespread permafrost vulnerability and soil active layer increases over the high northern latitudes inferred from satellite remote sensing and process model assessments," *Remote Sens. Environ.*, vol. 175, pp. 349–358, Mar. 2016.

[10] V. Naeimi *et al.*, "ASCAT surface state flag (SSF): Extracting information on surface Freeze/Thaw conditions from backscatter data using an empirical threshold-analysis algorithm," *IEEE Trans. Geosci. Remote Sens.*, vol. 50, no. 7, pp. 2566–2582, Jul. 2012.

[11] K. Rautiainen *et al.*, "Detection of soil freezing from L-band passive microwave observations," *Remote Sens. Environ.*, vol. 147, pp. 206–218, May 2014.

[12] T. Zhao, L. Zhang, L. Jiang, S. Zhao, L. Chai, and R. Jin, "A new soil freeze/thaw discriminant algorithm using AMSR-E passive microwave imagery," *Hydrol. Processes*, vol. 25, no. 11, pp. 1704–1716, Jan. 2011.

[13] S.-E. Park, A. Bartsch, D. Sabel, W. Wagner, V. Naeimi, and Y. Yamaguchi, "Monitoring freeze/thaw cycles using ENVISAT ASAR global mode," *Remote Sens. Environ.*, vol. 115, no. 12, pp. 3457–3467, Dec. 2011.

[14] V. Wismann, "Monitoring of seasonal thawing in siberia with ERS scatterometer data," *IEEE Trans. Geosci. Remote Sens.*, vol. 38, no. 4, pp. 1804–1809, Jul. 2000.

[15] S. Frolking, K. C. McDonald, J. S. Kimball, J. Way, R. Zimmermann, and S. W. Running, "Using the space-borne NASA scatterometer (NSCAT) to determine the frozen and thawed seasons," *J. Geophys. Res., Atmos.*, vol. 104, no. D22, pp. 27895–27907, 1999.

[16] J. Kimball, "Application of the NASA Scatterometer (NSCAT) for determining the daily frozen and nonfrozen landscape of Alaska," *Remote Sens. Environ.*, vol. 75, no. 1, pp. 113–126, Jan. 2001.

[17] C. Kroisleitner, A. Bartsch, and H. Bergstedt, "Circumpolar patterns of potential mean annual ground temperature based on surface state obtained from microwave satellite data," *Cryosphere*, vol. 12, no. 7, pp. 2349–2370, Jul. 2018. [Online]. Available: https://www.the-cryosphere.net/12/2349/2018/

[18] E. Rignot and J. B. Way, "Monitoring freezethaw cycles along north-south alaskan transects using ers-1 SAR," *Remote Sens. Environ.*, vol. 49, no. 2, pp. 131–137, 1994.

[19] M. Azarderakhsh, K. McDonald, H. Norouzi, A. Barros, P. Arunvavikul, and R. Blake, "Using Sentinel-L SAR measurements to detect high resolution freeze and thaw states in Alaska," in *Proc. IEEE Int. Geosci. Remote Sens. Symp. (IGARSS)*, Jul. 2018, pp. 2398–2399.

[20] N. Baghdadi, H. Bazzi, M. El Hajj, and M. Zribi, "Detection of frozen soil using Sentinel-1 SAR data," *Remote Sens.*, vol. 10, no. 8, p. 1182, Jul. 2018.

[21] H. Bergstedt and A. Bartsch, "Surface state across scales; temporal and spatial patterns in land surface Freeze/Thaw dynamics," *Geosciences*, vol. 7, no. 3, p. 65, Aug. 2017.

[22] X. Chen, L. Liu, and A. Bartsch, "Detecting soil freeze/thaw onsets in alaska using SMAP and ASCAT data," *Remote Sens. Environ.*, vol. 220, pp. 59–70, Jan. 2019. [Online]. Available: http://www.sciencedirect.com/science/article/pii/S0034425718304589

[23] K. Rautiainen *et al.*, "SMOS prototype algorithm for detecting autumn soil freezing," *Remote Sens. Environ.*, vol. 180, pp. 346–360, Jul. 2016. [Online]. Available: http://www.sciencedirect.com/science/article/pii/S0034425716300128

[24] Z. Bartalis *et al.*, "Initial soil moisture retrievals from the METOP—A Advanced Scatterometer (ASCAT)," *Geophys. Res. Lett.*, vol. 34, no. 20, pp. 1–5, Oct. 2007.

[25] J. Figa-Saldaña, J. J. W. Wilson, E. Attema, R. Gelsthorpe, M. R. Drinkwater, and A. Stoffelen, "The Advanced Scatterometer (ASCAT) on the meteorological operational (MetOp) platform: A follow on for European wind scatterometers," *Can. J. Remote Sens.*, vol. 28, no. 3, pp. 404–412, Jun. 2014.

[26] I. Nitze, G. Grosse, B. M. Jones, V. E. Romanovsky, and J. Boike, "Remote sensing quantifies widespread abundance of permafrost region disturbances across the arctic and subarctic," *Nature Commun.*, vol. 9, no. 1, p. 5423, Dec. 2018.

[27] L. Salzburg. *5 m, 10 m, 20 m, 100 m Contour Lines From ALS-DGM*. Accessed: 2016. [Online]. Available: https://www.data.gv.at/katalog/dataset/hohenlinien-des-landes-salzburg

[28] National Land Survey of Finland. *Elevation Model 10 m*. [Online]. Available: https://www.maanmittauslaitos.fi/en/maps-and-spatial-data/expert-users/product-descriptions/elevation-model-10-m

[29] *Sonnblick Observatory, Data Set Tawes 2 m Air Temperature*, Zentralanstalt für Meteorologie und Geodynamik, Vienna, Austria, 2019.

[30] M. Seppälä, "Depth of snow and frost on a Palsa mire, finnish lapland," *Geografiska Annaler. Ser. A, Phys. Geography*, vol. 72, no. 2, pp. 191–201, 1990.

[31] M. Seppälä, "An experimental climate change study of the effect of increasing snow cover on active layer formation of a palsa, finnish lapland," in *Proc. 8th Int. Conf. Permafrost*, vol. 2, 2003, pp. 1013–1016.

[32] B. Widhalm, A. Bartsch, and R. Goler, "Simplified normalization of C-Band synthetic aperture radar data for terrestrial applications in high latitude environments," *Remote Sens.*, vol. 10, no. 4, p. 551, Apr. 2018.

[33] A. Bartsch, B. Widhalm, G. Pointner, K. Ermokhina, M. Leibman, and B. Heim, "Landcover derived from Sentinel-1 and Sentinel-2 satellite data (2015–2018) for subarctic and arctic environments," *PANGAEA*, 2019, doi: 10.1594/PANGAEA.897916.

[34] A. Bartsch *et al.*, "Final report DUE-GlobPermafrost," Zentralanstalt für Meteorologie und Geodynamik, Vienna, Austria, Tech. Rep., 2019.

[35] E. Högström, A. Trofaier, I. Gouttevin, and A. Bartsch, "Assessing seasonal backscatter variations with respect to uncertainties in soil moisture retrieval in Siberian tundra regions," *Remote Sens.*, vol. 6, no. 9, pp. 8718–8738, Sep. 2014.

[36] E. Hogstrom and A. Bartsch, "Impact of backscatter variations over water bodies on coarse-scale radar retrieved soil moisture and the potential of correcting with meteorological data," *IEEE Trans. Geosci. Remote Sens.*, vol. 55, no. 1, pp. 3–13, Jan. 2017.

[37] R. D. Lindsley and D. G. Long, "Enhanced-resolution reconstruction of ASCAT backscatter measurements," *IEEE Trans. Geosci. Remote Sens.*, vol. 54, no. 5, pp. 2589–2601, May 2016.

Helena Bergstedt received the M.Sc. degree in geography from the Free University of Berlin, Berlin, Germany, in 2015, and the Ph.D. degree in applied geoinformatics from the Paris Lodron University of Salzburg, Salzburg, Austria, in 2019.

She is currently a Post-Doctoral Fellow with the Water and Environmental Research Center (WERC), Institute of Northern Engineering, University of Alaska Fairbanks, Fairbanks, AK, USA. Her research work focuses on remote sensing of permafrost landscapes and spatial heterogeneities of surface processes.

Annett Bartsch received the M.Sc. degree from the Friedrich-Schiller University of Jena, Jena, Germany, in 2000, and the Ph.D. degree in geography from the University of Reading, Reading, U.K., in 2004.

Since 2003, she has been with the Vienna University of Technology, Vienna, Austria. She has been teaching at the University of Salzburg, Salzburg, Austria, since 2012. From 2014 to 2016, she was the Head of the Climate Change Impacts Section, Zentralanstalt für Meteorologie und Geodynamik (ZAMG), Vienna. She is currently the Managing Director of b.geos, Korneuburg, Austria, and she is also a member of the Austrian Polar Research Institute, Vienna. She focuses on the application of satellite data at high-latitudes related to land surface hydrology and for interdisciplinary studies. Her research interests include active microwave remote sensing techniques for analyses of frozen ground, wetlands, lakes, and snow.

Anton Neureiter received the B.Sc. degree in geography from the University of Vienna, Vienna, Austria, in 2019.

Since 2011, he has been a member of the Department for Climate Research, Climate Monitoring and Cryosphere Section, Zentralanstalt für Meteorologie und Geodynamik (ZAMG), Vienna. He focuses on glacier mass balance and permafrost measurements.

Angelika Höfler received the Ph.D. degree in mathematics from the Faculty of Mathematics, University of Vienna, Vienna, Austria, in 2014.

From 2010 to 2014, she worked as a Research Assistant at the Faculty of Mathematics, University of Vienna. Since 2014, she has been contributing to several projects of the Climate Research Department, Zentralanstalt für Meteorologie und Geodynamik (ZAMG), Vienna. In 2016, she joined the Climate Change Impacts Section, ZAMG, where she was involved in the processing of Sentinel-1 data and the application of satellite data for climate impact research. She is currently a trained mathematician with a strong interest in climate research.

Barbara Widhalm received the Dipl.Ing (M.Sc.) degree and the Dr.Techn. (Ph.D.) degree in geodesy and geoinformation from the Vienna University of Technology, Vienna, Austria, in 2013 and 2018, respectively.

From 2013 to 2015, she worked as a Project Assistant at the Department of Photogrammetry and Remote Sensing, Vienna University of Technology. Since 2015, she has been working at the Zentralanstalt für Meteorologie und Geodynamik (ZAMG), Vienna, where she has also been with the Climate Change Impacts Section and currently with the Staff Unit Earth Observation. Her research work includes the study of Arctic permafrost by integrating Earth observation data. She focuses on the determination of Arctic land surface and soil properties with synthetic aperture radar data.

Nicholas Pepin received the Ph.D. degree in geography from the University of Durham, Durham, U.K., in 1994, studying patterns of warming in the mountains of the U.K.

He is currently a Reader of climate science with the University of Portsmouth, Portsmouth, U.K. He combines a field-based approach with remote sensing and modeling to investigate changing patterns of elevation-dependent warming across varied mountain regions. His field networks include Kilimanjaro, Finnish Lapland, and the Pyrenees.

Jan Hjort received the Ph.D. degree in geography from the University of Helsinki, Helsinki, Finland, in 2006.

He is currently a Professor of physical geography with the Geography Research Unit, University of Oulu, Oulu, Finland. His research interests include permafrost and periglacial processes, biodiversity–geodiversity relationships, and environmental risk assessments in the Arctic, Boreal, and Alpine environments. Methodologically, the main approach is geospatial data-based statistical analysis.